GENERAL

Design and implementation of a novel multi-scroll chaotic system

Vol 18 No 1, January 2009
1674-1056/2009/18(01)/0119-11

Chinese Physics B

Design and implementation of a novel multi-scroll chaotic system*

Zhang Chao-Xia(张朝霞) and Yu Si-Min (禹思敏)†

College of Automation, Guangdong University of Technology, Guangzhou 510006, *China*

(Received 9 July 2008; revised manuscript received 8 August 2008)

This paper proposes a novel approach for generating a multi-scroll chaotic system. Together with the theoretical design and numerical simulations, three different types of attractor are available, governed by constructing triangular wave, sawtooth wave and hysteresis sequence. The presented new multi-scroll chaotic system is different from the classical multi-scroll chaotic Chua system in dimensionless state equations, nonlinear functions and maximum Lyapunov exponents. In addition, the basic dynamical behaviours, including equilibrium points, eigenvalues, eigenvectors, eigenplanes, bifurcation diagrams and Lyapunov exponents, are further investigated. The success of the design is illustrated by both numerical simulations and circuit experiments.

Keywords: multi-scroll chaotic attractors, triangular and sawtooth waves, hysteresis sequence, circuit implementation

PACC: 0545

1. Introduction

Since the discovery of the Lorenz system by the eminent scholar Lorenz during his study in 1963, the famous butterfly attractor has become a paradigm in chaos.[1−3] In 1984, Chua presented the first chaotic circuit, which builds a connection between the chaos theory and the nonlinear circuit.[4]

In recent years, based on Lorenz, Chua and other systems, different types of multi-scroll chaotic systems have been designed and implemented,[5−28] such as the multi-scroll Chua system,[5−13] multi-scroll Jerk system,[14,15] multi-folded torus system,[16,17] grid multi-torus system,[18] grid multi-scroll Chua system,[19] multi-directional multi-scroll chaotic system,[20−25] ring-shaped multi-scroll generalized Lorenz system,[26] and so on. However, chaotic systems which can generate multiple scrolls are still very restricted.[27]

In this paper, a novel multi-scroll chaotic system is proposed on the basis of the classical multi-scroll Chua system.[4,8−12] It is confirmed that three different types of multiple scroll chaotic attractors are available by constructing triangular wave, sawtooth wave and hysteresis sequence. Furthermore, its generating mechanism and dynamical behaviours are investigated and the circuit experimental results are also given.

The paper is organized as follows. The novel multi-scroll chaotic system is presented in Section 2. The basic dynamical behaviours for multi-scroll chaotic attractors are analysed in Section 3. A module-based circuit is designed in Section 4 and circuit implementation results are demonstrated in Section 5. Finally, conclusions are given in Section 6.

2. A novel multi-scroll chaotic system

The new chaotic system is given as below:

$$\begin{aligned} \dot{x} &= \beta\, y - x - \alpha\, f(x), \\ \dot{y} &= \beta\, x - \gamma\, z, \\ \dot{z} &= \xi\, y - z, \end{aligned} \tag{1}$$

where $\alpha = 4.2$, $\beta = 6.7$, $\gamma = 4.0$, ξ is a control parameter and $f(x)$ is a nonlinear function.

It should be emphasized that the dimensionless state equation expressed as Eq.(1) is different from that expressed in the classical Chua system, although they both provide scroll-like attractors. Recall the

*Project supported by the National Natural Science Foundation of China (Grant Nos 60572073 and 60871025) and the Natural Science Foundation of Guangdong Province, China (Grant Nos 8151009001000060, 5001818 and 8351009001000002).

†E-mail: siminyu@163.com

Chua system [4,8−12]

$$\begin{aligned}\dot{x} &= \alpha\,[y - f(x)],\\ \dot{y} &= x - y + z,\\ \dot{z} &= -\beta y + \gamma\, z,\end{aligned} \tag{2}$$

where $\alpha = 10$, $\beta = 15$, $\gamma = 0.04$ and $f(x)$ is a nonlinear function.

The following differences are noticed:

1) The second state equations in Eqs.(1) and (2) are different, which leads to different equilibrium points and attractor's topology;

2) The nonlinear function $f(x)$ of Eq.(2) is piecewise-linear or sinusoidal, while $f(x)$ of Eq.(1) is triangular wave, sawtooth wave or hysteresis function;

3) The maximum Lyapunov exponents of Eq.(1) can be larger than 1.2, while those of Eq.(2) are normally less than 0.3, as presented in the later sections.

2.1. Generating multi-scroll chaotic attractors using triangular wave

Let the nonlinear function $f(x)$ in Eq.(1) be a triangular wave. To generate $2N$ ($N \geq 1$) scrolls, $f(x)$ is in the form of

$$\begin{aligned}f(x) &= f_1(x)\\ &= x + \sum_{n=1}^{2N-1} (-1)^n [|x + (2n-1)|\\ &\quad - |x - (2n-1)|].\end{aligned} \tag{3}$$

To generate $2N+1$ ($N \geq 1$) scrolls, $f(x)$ is expressed as

$$\begin{aligned}f(x) &= f_2(x)\\ &= x + \sum_{n=1}^{2N} (-1)^{n-1} [|x + (2n-1)|\\ &\quad - |x - (2n-1)|].\end{aligned} \tag{4}$$

Note that the number of scrolls is related to parameter ξ in Eq.(1). Let N be a positive integer and ξ be a variable. According to Eqs.(1) and (3), the number of scrolls is $2M$ ($1 \leq M \leq N$) and the maximum number of scrolls is $2N$. Similarly, based on Eqs.(1) and (4), the number of scrolls is $2M+1$ ($1 \leq M \leq N$) and the maximum number of scrolls is $2N+1$. The relationship among N, ξ and the maximum number of scrolls is given in Tables 1 and 2 for even scrolls and odd scrolls, respectively.

Table 1. Relationship among N, ξ, and maximum number of even scrolls from a triangular wave system.

N	1	2	3	4	5
ξ	18.5	13.0	12.2	11.8	11.6
maximum number of scrolls	2	4	6	8	10

Table 2. Relationship among N, ξ, and maximum number of odd scrolls from a triangular wave system.

N	1	2	3	4
ξ	14.0	12.6	12.0	11.7
maximum number of scrolls	3	5	7	9

According to Eqs.(1), (3), (4) and Tables 1 and 2, the numerical simulation results of 9- and 10-scroll chaotic attractors are depicted in Fig.1. Different from the classical Chua system, the main feature of the new chaotic system is that scrolls with mutual nesting topologically are surrounded by outer phase trajectory.

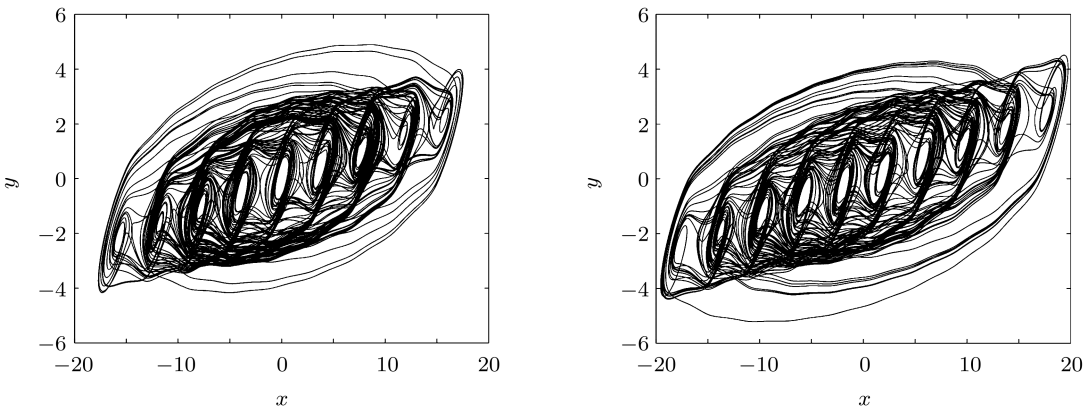

(a) 9-scroll chaotic attractor (b) 10-scroll chaotic attractor

Fig.1. 9- and 10-scroll chaotic attractors generated from a triangular wave system.

2.2. Generating multi-scroll chaotic attractors using sawtooth wave

Let the nonlinear function $f(x)$ in Eq.(1) be a sawtooth wave. To generate $2N$ $(N \geq 1)$ scrolls, $f(x)$ is written as

$$\begin{aligned} f(x) &= f_1(x) \\ &= x - \sum_{n=0}^{N-1} \operatorname{sgn}(x+2n) \\ &\quad - \sum_{n=1}^{N-1} \operatorname{sgn}(x-2n). \end{aligned} \tag{5}$$

To generate $2N+1$ $(N \geq 1)$ scrolls, $f(x)$ is expressed as

$$\begin{aligned} f(x) &= f_2(x) \\ &= x - \sum_{n=1}^{N} \operatorname{sgn}[x+(2n-1)] \\ &\quad - \sum_{n=1}^{N} \operatorname{sgn}[x-(2n-1)]. \end{aligned} \tag{6}$$

Let N be a positive integer and ξ be a variable. Based on Eqs.(1) and (5), the number of scrolls is $2M$ $(1 \leq M \leq N)$ and the maximum number is $2N$. Similarly, based on Eqs.(1) and (6), the number of scrolls is $2M+1$ $(1 \leq M \leq N)$ and the maximum number of scrolls is $2N+1$. The relationship among N, ξ and the maximum number of scrolls is given in Tables 3 and 4 for even scrolls and odd scrolls, respectively. The numerical simulation results of 7- and 8-scroll chaotic attractors are depicted in Fig.2.

Table 3. Relationship among N, ξ, and maximum number of even scrolls from a sawtooth wave system.

N	1	2	3	4	5
ξ	25.0	15.5	13.4	12.5	12.2
maximum number of scrolls	2	4	6	8	10

Table 4. Relationship among N, ξ, and maximum number of odd scrolls in a sawtooth wave system.

N	1	2	3	4
ξ	17.0	14.0	13.0	12.3
maximum number of scrolls	3	5	7	9

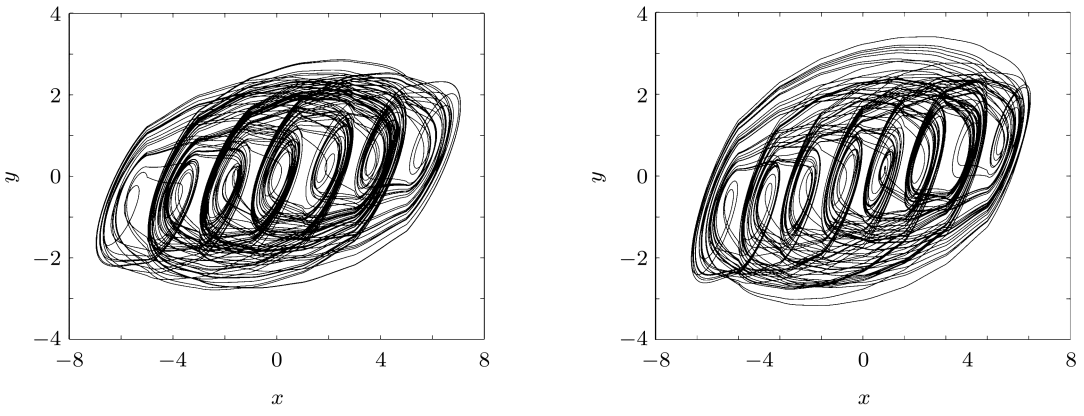

(a) 7-scroll chaotic attractor (b) 8-scroll chaotic attractor

Fig.2. 7- and 8-scroll chaotic attractors generated from a sawtooth wave system.

2.3. Generating multi-scroll chaotic attractors using hysteresis sequence

The basic hysteresis functions are defined as

$$h_0(x) = \begin{cases} -1, & \text{if} \quad x < -1, \\ +1, & \text{if} \quad x > +1, \end{cases}$$

$$h_{-n}(x+2n) = \begin{cases} -2, & \text{if} \quad x+2n < -1, \\ 0, & \text{if} \quad x+2n > +1, \end{cases}$$

$$h_{+n}(x-2n) = \begin{cases} 0, & \text{if} \quad x-2n < -1, \\ 2, & \text{if} \quad x-2n > +1. \end{cases} \tag{7}$$

Let the nonlinear function $f(x)$ be a hysteresis sequence in Eq.(1). To create $(2+N+M)$ scrolls, $f(x)$ is expressed as

$$f(x) = x - h_0(x) - \sum_{n=1}^{N} [h_{+n}(x-2n)]$$

$$-\sum_{n=1}^{M}[h_{-n}(x+2n)], \tag{8}$$

where $N, M \geq 0$. The relationship among N, ξ, M and the maximum number of scrolls is given in Tables 5 and 6. According to Eqs.(1), (8) and Table 6, the numerical simulation results of 13- and 14-scroll chaotic attractors are depicted in Fig.3.

Table 5. Relationship among N, ξ, M, and maximum number of scrolls from a hysteresis system.

N	0	1	1	2	2	3	3
M	0	0	1	1	2	2	3
ξ	28.0	22.0	18.0	15.8	14.8	14.0	13.0
maximum number of scrolls	2	3	4	5	6	7	8

Table 6. Relationship between N, ξ, M, and maximum number of scrolls from a hysteresis system (continued).

N	4	4	5	5	6	6
M	3	4	4	5	5	6
ξ	12.8	12.5	12.2	12.0	11.85	11.8
maximum number of scrolls	9	10	11	12	13	14

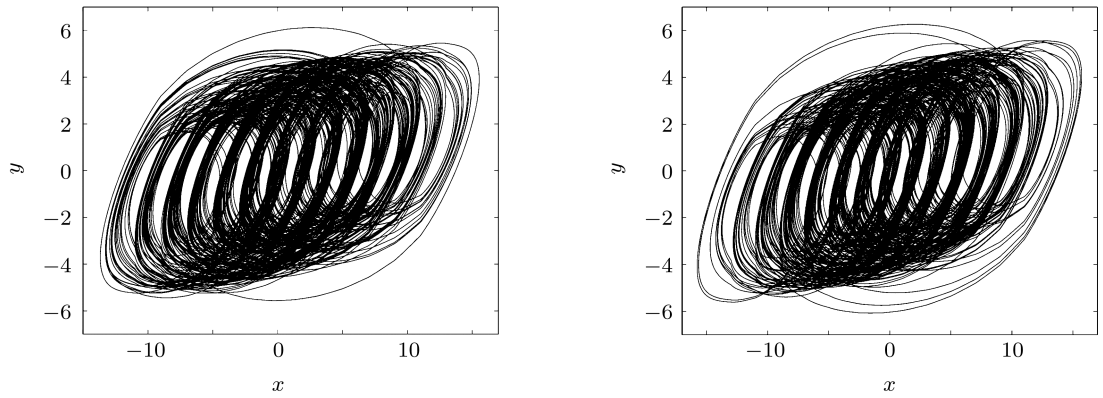

(a) 13-scroll chaotic attractor (b) 14-scroll chaotic attractor

Fig.3. 13- and 14-scroll chaotic attractors generated from a hysteresis sequence.

3. Basic dynamical behaviours

In this section, some basic dynamical behaviours, including equilibrium points, eigenvalues, eigenvectors, eigenplanes, maximum Lyapunov exponents and bifurcations, are further investigated to confirm the existence of chaos of Eq.(1).

Let $\dot{x} = 0$, $\dot{y} = 0$, $\dot{z} = 0$. According to Eq.(1), equilibrium point equations are obtained

$$\begin{aligned} f(x) &= [\beta^2/(\gamma\xi) - 1]x/\alpha, \\ y &= \beta x/(\gamma\xi), \\ z &= \beta x/\gamma. \end{aligned} \tag{9}$$

By solving Eq.(9), equilibrium points can be calculated and determined.

3.1. Equilibrium points and eigenvalues

Let nonlinear function $f(x)$ be a triangular wave. According to Eqs.(3), (4) and (9), equilibrium points $Q^{\pm n}(x^{\pm n}, y^{\pm n}, z^{\pm n})$ of 9- and 10-scroll attractors are depicted in Fig.4, where 'O' and 'X' stand for the first and second type of equilibrium points, respectively.

Based on Eqs.(4) and (9), to create $2N+1$ ($N \geq 1$) scrolls, the solution of equilibrium points in Eq.(1) can be determined by

$$\begin{aligned} x^{\pm n} &= \pm\frac{2\alpha n}{[1-\beta^2/(\gamma\xi)] + (-1)^n\alpha}, \\ y^{\pm n} &= \frac{\beta}{\gamma\xi}x^{\pm n}, \\ z^{\pm n} &= \frac{\beta}{\gamma}x^{\pm n}, \end{aligned} \tag{10}$$

where $0 \le n \le 2N$. Let $N = 4$. According to Eq.(10), equilibrium points of 9-scroll chaotic attractors are depicted in Fig.4(a). Similarly, based on Eqs.(3) and (9), to generate $2N$ ($N \ge 1$) scrolls, the solution of equilibrium points in Eq.(1) can be expressed as follows:

$$x^{\pm n} = \pm \frac{2\alpha n}{[1-\beta^2/(\gamma\xi)] + (-1)^{n+1}\alpha},$$
$$y^{\pm n} = \frac{\beta}{\gamma\xi} x^{\pm n},$$
$$z^{\pm n} = \frac{\beta}{\gamma} x^{\pm n}, \tag{11}$$

where $0 \le n \le 2N-1$. Let $N = 5$. According to Eq.(11), equilibrium points of 10-scroll chaotic attractors are depicted in Fig.4(b).

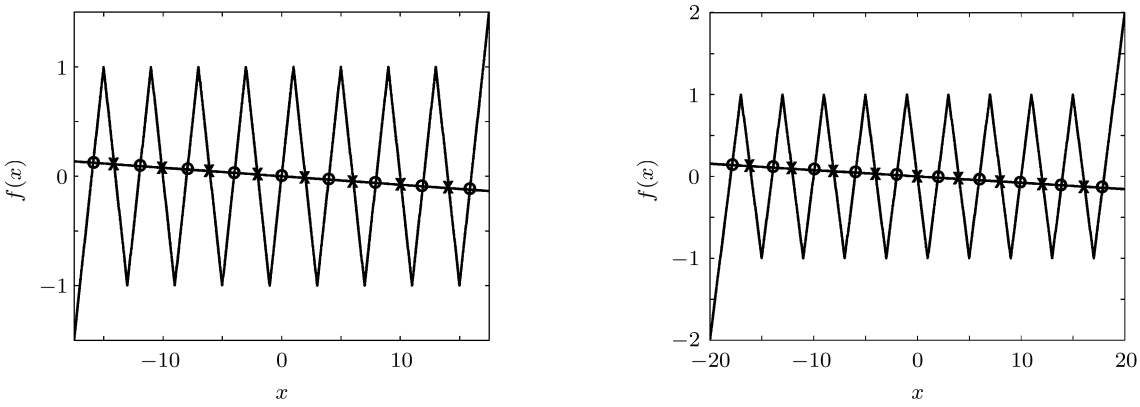

(a) equilibrium points of 9-scroll (b) equilibrium points of 10-scroll

Fig.4. Equilibrium points of 9- and 10-scroll generated from a triangular wave system.

Let nonlinear function $f(x)$ be a sawtooth wave. According to Eqs.(5), (6) and (9), the solution for the first type of equilibrium points can be obtained as follows:

$$x^{\pm n} = \pm \frac{\{2n + 0.5[1+(-1)^L]\}\alpha}{[1-\beta^2/(\gamma\xi)] + \alpha},$$
$$y^{\pm n} = \frac{\beta}{\gamma\xi} x^{\pm n},$$
$$z^{\pm n} = \frac{\beta}{\gamma} x^{\pm n}, \tag{12}$$

where $n \ge 0$, $L \ge 2$, L is the number of scrolls. Similarly, the solution for the second type of equilibrium points can be solved by $x^{\pm n} = \pm\{2n+0.5[1-(-1)^L]\}$, $y^{\pm n} = \beta x^{\pm n}/(\gamma\xi)$, $z^{\pm n} = \beta x^{\pm n}/\gamma$. For example, equilibrium points of 7- and 8-scroll created by a sawtooth wave are depicted in Fig.5, where 'O' and 'X' stand for the first and second type of equilibrium points, respectively.

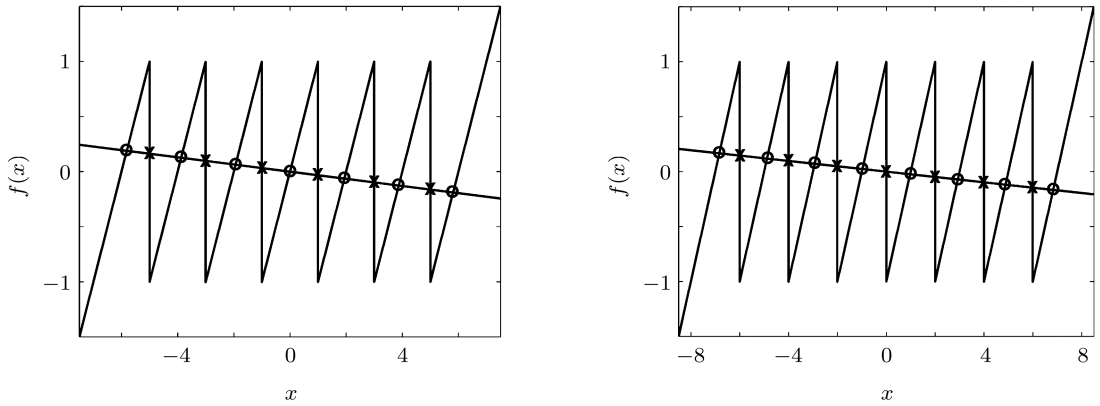

(a) equilibrium points of 7-scroll (b) equilibrium points of 8-scroll

Fig.5. Equilibrium points of 7- and 8-scroll generated from a sawtooth wave system.

Let nonlinear function $f(x)$ be a hysteresis sequence in Eq.(9). Equilibrium points of 13- and 14-scroll are depicted in Fig.6, where 'O' stands for the first type of equilibrium points, calculated by Eq.(12) for the case of L being positive even numbers. The second type of equilibrium points can be determined by $x^{\pm n} = \pm(2n-1)$, $y^{\pm n} = \beta x^{\pm n}/(\gamma\xi)$, $z^{\pm n} = \beta x^{\pm n}/\gamma$, where $n \geq 1$.

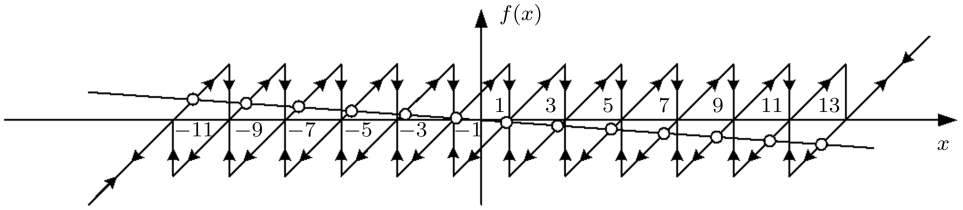

(a) equilibrium points of 13-scroll generated from hysteresis sequence

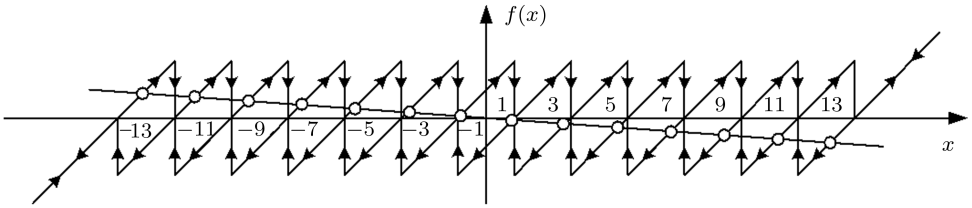

(b) equilibrium points of 14-scroll generated from hysteresis sequence

Fig.6. Equilibrium points of 13- and 14-scroll generated from hysteresis sequences.

In the following, we take the triangular wave as an example and calculate eigenvalues of equilibrium points. Based on Eq.(1), the linearized Jacobian matrix is obtained as follows:

$$\boldsymbol{J}_{\mathrm{P}} = \begin{bmatrix} -1-\alpha f'(P) & \beta & 0 \\ \beta & 0 & -\gamma \\ 0 & \xi & -1 \end{bmatrix}, \tag{13}$$

where $f(x)$ is a triangular wave, $f'(P) = \pm 1$, $\alpha = 4.2$, $\beta = 6.7$, $\gamma = 4.0$.

Let $\xi = 11.6$. According to Eq.(13), the associated eigenvalues for the first type of equilibrium points are obtained, $\lambda_1 = -8.2638$, $\sigma_1 \pm \mathrm{j}\omega_1 = 1.0319 \pm \mathrm{j}4.7645$, and those for the second type of equilibrium points are $\lambda_2 = 6.7259$, $\sigma_2 \pm \mathrm{j}\omega_2 = -2.2629 \pm \mathrm{j}4.8610$. Hence, it is confirmed that the first type of equilibrium points are saddle-focus ones with index-2, while the second type of equilibrium points are saddle-focus ones with index-1.

3.2. Eigenvectors and eigenplanes

According to $(\lambda E - \boldsymbol{J}_{\mathrm{P}})\boldsymbol{v} = 0$, the corresponding real eigenvectors $\boldsymbol{v} = [v_1 \ v_2 \ v_3]^{\mathrm{T}}$ of real eigenvalue λ created from the triangular wave are expressed as

$$\begin{bmatrix} \lambda+1+\alpha f'(P) & -\beta & 0 \\ -\beta & \lambda & \gamma \\ 0 & -\xi & \lambda+1 \end{bmatrix} \begin{bmatrix} v_1 \\ v_2 \\ v_3 \end{bmatrix} = 0. \tag{14}$$

Let $v_3 = \xi$. Based on Eq.(14), one of real eigenvectors is obtained

$$[v_1 \ v_2 \ v_3]^{\mathrm{T}} = [(\lambda^2+\lambda+\xi\gamma)/\beta \quad \lambda+1 \quad \xi]^{\mathrm{T}}. \tag{15}$$

Using Eq.(15), the spatial linear equation of corresponding eigenvector of λ is given by

$$\frac{x-x_{\mathrm{Q}}}{(\lambda^2+\lambda+\xi\gamma)/\beta} = \frac{y-y_{\mathrm{Q}}}{\lambda+1} = \frac{z-z_{\mathrm{Q}}}{\xi}. \tag{16}$$

The associated complex eigenvectors $\tilde{\boldsymbol{v}} = [\tilde{v}_1 \ \tilde{v}_2 \ \tilde{v}_3]^{\mathrm{T}}$ of complex conjugate eigenvalue can be obtained as follows:

$$\begin{bmatrix} \sigma+\mathrm{j}\,\omega+1+\alpha f'(Q) & -\beta & 0 \\ -\beta & \sigma+\mathrm{j}\,\omega & \gamma \\ 0 & -\xi & \sigma+\mathrm{j}\,\omega+1 \end{bmatrix} \begin{bmatrix} \tilde{v}_1 \\ \tilde{v}_2 \\ \tilde{v}_3 \end{bmatrix} = 0. \tag{17}$$

Let $\tilde{v}_3 = \xi$. From Eq.(17), one of complex eigenvectors can expressed as

$$\begin{bmatrix} \tilde{v}_1 \\ \tilde{v}_2 \\ \tilde{v}_3 \end{bmatrix} = \begin{bmatrix} ((\sigma+\mathrm{j}\,\omega)(\sigma+\mathrm{j}\,\omega+1)+\gamma\xi)/\beta \\ \sigma+\mathrm{j}\,\omega+1 \\ \xi \end{bmatrix}$$

$$= \begin{bmatrix} (\sigma^2+\sigma(2\omega+1)+\gamma\xi)/\beta + \mathrm{j}(\omega-\omega^2)/\beta \\ (\sigma+1)+\mathrm{j}\,\omega \\ \xi \end{bmatrix}. \tag{18}$$

Using real part and imaginary part of complex eigenvector denoted by Eq.(18), two new vectors are obtained:

$$\begin{aligned} \boldsymbol{\varsigma}_1 &= [(\sigma^2+\sigma(2\omega+1)+\gamma\xi)/\beta \quad (\sigma+1) \quad \xi], \\ \boldsymbol{\varsigma}_2 &= [(\omega-\omega^2)/\beta \quad \omega \quad 0]. \end{aligned} \tag{19}$$

An eigenplane $(\boldsymbol{\varsigma}_1, \boldsymbol{\varsigma}_2)$ can be spanned by vectors $\boldsymbol{\varsigma}_1$ and $\boldsymbol{\varsigma}_2$:

$$\begin{aligned} \boldsymbol{\varsigma}_1 \times \boldsymbol{\varsigma}_2 &= \left\{ \begin{vmatrix} (\sigma+1) & \xi \\ \omega & 0 \end{vmatrix}, \begin{vmatrix} \xi & (\sigma^2+\sigma(2\omega+1)+\gamma\xi)/\beta \\ 0 & (\omega-\omega^2)/\beta \end{vmatrix}, \begin{vmatrix} (\sigma^2+\sigma(2\omega+1)+\gamma\xi)/\beta & (\sigma+1) \\ (\omega-\omega^2)/\beta & \omega \end{vmatrix} \right\} \\ &= \left\{ -\xi\omega, \quad \xi(\omega-\omega^2)/\beta, \quad \omega(\sigma^2+\sigma(2\omega+1)+\gamma\xi)/\beta - (\sigma+1)(\omega-\omega^2)/\beta \right\}. \end{aligned} \tag{20}$$

Finally, the corresponding eigenplane equation of complex conjugate eigenvalue can be obtained as below:

$$A(x-z_{\mathrm{Q}}) + B(y-y_{\mathrm{Q}}) + C(z-z_{\mathrm{Q}}) = 0, \tag{21}$$

where $A = -\xi\omega$, $B = \xi(\omega-\omega^2)/\beta$, $C = \omega(\sigma^2+\sigma(2\omega+1)+\gamma\xi)/\beta - (\sigma+1)(\omega-\omega^2)/\beta$.

3.3. Generation mechanism analysis of multi-scroll chaotic attractors

Since the generation mechanism of multiple scrolls is similar for different numbers of scrolls, only 3-scroll is considered. Referring to Eq.(10) for the case of $N = 1$, five equilibrium points can be obtained as follows:

$$\begin{cases} O(0,0,0), \\ P^{\pm1}(\pm 2.0156, \pm 0.2910, \pm 3.3762), \\ P^{\pm2}(\pm 3.9692, \pm 0.5731, \pm 6.6485). \end{cases} \tag{22}$$

The five equilibrium points are plotted in Fig.7. As mentioned in the last section, equilibrium points O, $P^{\pm2}$ are saddle-focus ones with index-2, generating scrolls by axial direction shrinkage and radial direction tension in the corresponding regions D_{-2}, D_0, D_{+2}, respectively. While equilibrium points $P^{\pm1}$ are saddle-focus ones with index-1, forming bond orbits by axial direction tension and radial direction shrinkage in the corresponding regions D_{-1} and D_{+1}, respectively.

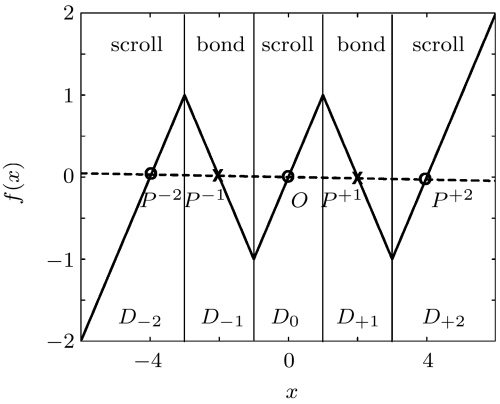

Fig.7. Five equilibrium points and their corresponding regions.

Letting $\alpha = 4.2$, $\beta = 6.7$, $\gamma = 4.0$, $\xi = 11.6$, one has $\lambda = \lambda_1 = -8.2638$, $\sigma \pm \mathrm{j}\,\omega = \sigma_1 \pm \mathrm{j}\,\omega_1 = 1.0319 \pm \mathrm{j}\,4.7645$. From Eqs.(16) and (21), the corresponding eigenvector equations and eigenplane equations for the first type of equilibrium points $O(0,0,0)$ can be obtained as follows:

$$\begin{aligned} &E^{\mathrm{S}}(O): \frac{x}{15.8846} = \frac{y}{-7.2638} = \frac{z}{11.6000}, \\ &E^{\mathrm{U}}(O): -55.2682x - 31.0533y + 46.9188z = 0. \end{aligned} \tag{23}$$

The associated eigenvector equations and eigenplane equations for the first type of equilibrium points $P^{\pm2}(\pm 3.9692, \pm 0.5731, \pm 6.6485)$ are given below:

$$\begin{aligned} E^{\mathrm{S}}(P^{\pm2}): \ & \frac{x \pm 3.9692}{15.8846} = \frac{y \pm 0.5731}{-7.2638} = \frac{z \pm 6.6485}{11.6000}, \\ E^{\mathrm{U}}(P^{\pm2}): \ & -55.2682(x \pm 3.9692) \\ & -31.0533(y \pm 0.5731) \\ & +46.9188(z \pm 6.6485) = 0. \end{aligned} \tag{24}$$

Similarly, letting $\alpha = 4.2$, $\beta = 6.7$, $\gamma = 4.0$, $\xi = 11.6$, one has $\lambda = \lambda_2 = 6.7259$, $\sigma \pm \mathrm{j}\omega = \sigma_2 \pm \mathrm{j}\,\omega_2 = -2.2629 \pm \mathrm{j}\,4.8610$. According to Eqs.(16) and (21), the corresponding eigenvector equations and eigenplane equations for the second type of equilibrium points $P^{\pm 1}(\pm 2.0156, \pm 0.2910, \pm 3.3762)$ can be obtained as follows:

$$\begin{aligned} E^{\mathrm{U}}(P^{\pm 1}):\ & \frac{x \pm 2.0156}{14.6811} = \frac{y \pm 0.2910}{7.7259} = \frac{z \pm 3.3762}{11.6000}, \\ E^{\mathrm{S}}(P^{\pm 1}):\ & -56.3876(x \pm 2.0156) \\ & -32.4944(y \pm 0.2910) \\ & +16.2385(z \pm 3.3762) = 0. \end{aligned} \tag{25}$$

Using Eqs.(22)–(25), the corresponding eigenplanes and eigenvectors for the five equilibrium points O, $P^{\pm 1}$, $P^{\pm 2}$ and their spanned three-dimensional feature space are depicted in Fig.8. It is clearly seen that $E^{\mathrm{S}}(P^{-2})$, $E^{\mathrm{S}}(O)$ and $E^{\mathrm{S}}(P^{+2})$ are stable manifolds, while $E^{\mathrm{U}}(P^{-2})$, $E^{\mathrm{U}}(O)$ and $E^{\mathrm{U}}(P^{+2})$ are unstable manifolds. With the interaction of both stable manifolds and unstable manifolds, the equilibrium points O and $P^{\pm 2}$ generate three scrolls by axial direction shrinkage and radial direction tension in the corresponding regions D_{-2}, D_0 and D_{+2}, respectively. Similarly, $E^{\mathrm{S}}(P^{-1})$ and $E^{\mathrm{S}}(P^{+1})$ are stable manifolds, while $E^{\mathrm{U}}(P^{-1})$ and $E^{\mathrm{U}}(P^{+1})$ are unstable manifolds. With the interaction of both stable manifolds and unstable manifolds, equilibrium points $P^{\pm 1}$ form bond orbits by axial direction tension and radial direction shrinkage in the corresponding regions D_{-1} and D_{+1}, respectively. Finally, 3-scroll chaotic attractor can be created by connecting phase trajectories between bond orbits and scrolls. The generation mechanism is also suitable for creating n ($n > 3$) scroll chaotic attractors.

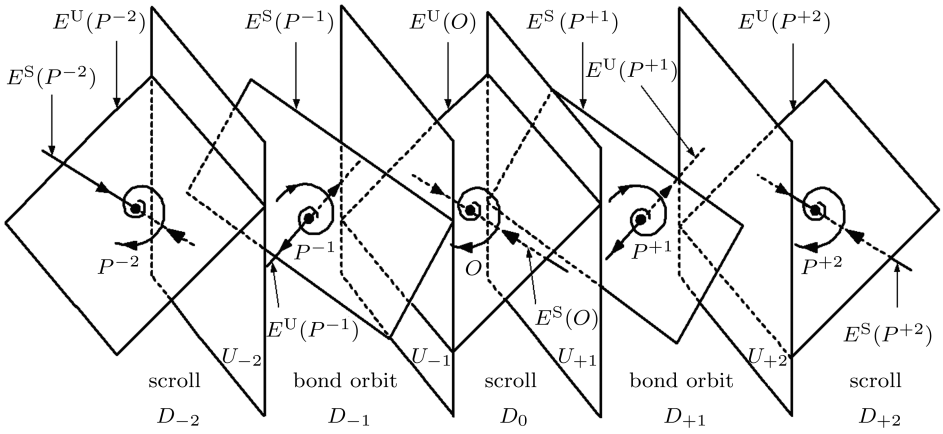

Fig.8. Corresponding eigenplanes, eigenvectors and their spanned 3-D feature space.

3.4. Bifurcation diagram and Lyapunov exponent

In the following, we take the triangular wave as an example and confirm the existence of chaos in Eq.(1). The bifurcation diagram of parameter ξ is obtained and depicted in Fig.9. A clear route from periodic oscillations to chaos is observed. The maximum Lyapunov exponent (LE) spectra is also obtained and depicted in Fig.10. The existence of positive LE indicates the chaotic nature of the system. Moreover, one can see from Fig.10 that the maximum Lyapunov exponents can be larger than 1.2, while those of Chua's system are normally less than 0.3.

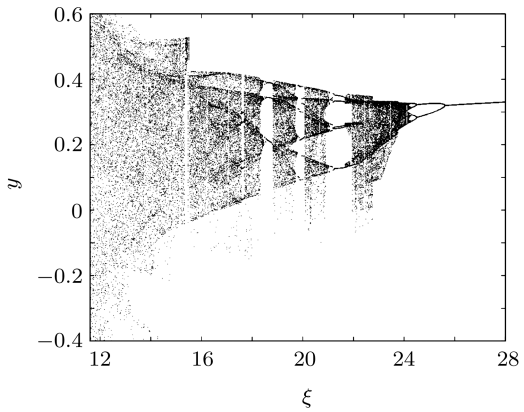

Fig.9. Bifurcation diagram.

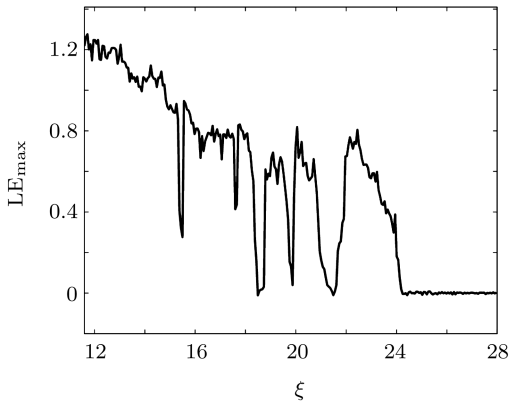

Fig.10. Maximum LE spectrum of Eq.(1) as a function of ξ.

4. Module-based circuit design

Based on dimensionless state equations and the module-based method,[28] Eq.(1) can be converted to actual circuit state equations and realized by circuit design using triangular wave.

First, it is necessary to take into account variable-scale reduction when the state variables exceed the linear dynamic range of active devices determined by saturation value. In this design, the power supply for all operational amplifiers of type TL082 is ±15V, and the saturation value for all operational amplifiers is ±13.5V. According to Fig.1, variable-scale reduction is expected.

Second, compared with in-phase addition and subtraction operational circuits, the parameters of reversed-phase addition and subtraction operational circuits are independently adjustable and convenient to tune, which is more suitable for module-based design.

Finally, actual circuit state equations can be obtained by differential to integral conversion and transformation of time-scale from Eq.(1).

Let variable-scale reduction factor be 1/5. After some simplified treatment, Eq.(1) is invariable under transformation, while Eqs.(3) and (4) are transferred as follows:

$$f(x)=\begin{cases} x+\sum\limits_{n=1}^{2N-1}(-1)^n[|x+(2n-1)/5|-|x-(2n-1)/5|], \\ x+\sum\limits_{n=1}^{2N}(-1)^{n-1}[|x+(2n-1)/5|-|x-(2n-1)/5|]. \end{cases} \tag{26}$$

Let $\tau = t/\tau_0$. By differential to integral conversion and transformation of time-scale, Eq.(1) is transferred as below:

$$\begin{aligned} x &= \frac{1}{R_0C_0}\int[-\beta(-y)-x-\alpha\, f(x)]\,\mathrm{d}t, \\ y &= \frac{1}{R_0C_0}\int[-\beta(-x)-\gamma\, z]\,\mathrm{d}t, \\ z &= \frac{1}{R_0C_0}\int[-\xi(-y)-z]\,\mathrm{d}t, \end{aligned} \tag{27}$$

where $R_0 = 50\,\mathrm{k\Omega}$, $C_0 = 50\,\mathrm{nF}$, $\tau_0 = R_0C_0$ is the transformation factor of time-scale. Using Eq.(27), one can design the circuit diagram as shown in Fig.11. The realization of $f(x)$ is depicted in Fig.12. In Figs.11 and 12, all operational amplifiers are TL082, and resistances are precisely adjustable. The relationship among resistors R in Fig.11, switch positions in Fig.12, and number of scrolls is given in Tables 7 and 8. The values of resistances in Fig.12 are further determined as follows:

1) When the number of scrolls is $2N$ ($N \geq 1$), one has $R_{i1}(2 \leq i \leq 19) = 1\,\mathrm{k\Omega}$, $R_{22} = 3.97\,\mathrm{k\Omega}$, $R_{42} = 3.5\,\mathrm{k\Omega}$, $R_{62} = 5.19\,\mathrm{k\Omega}$, $R_{82} = 5.14\,\mathrm{k\Omega}$, $R_{102} = 7.5\,\mathrm{k\Omega}$, $R_{122} = 8.64\,\mathrm{k\Omega}$, $R_{142} = 13.5\,\mathrm{k\Omega}$, $R_{162} = 21.5\,\mathrm{k\Omega}$, $R_{182} = 67.5\,\mathrm{k\Omega}$, $R_{32} = 0.99\,\mathrm{k\Omega}$, $R_{52} = 1.25\,\mathrm{k\Omega}$, $R_{72} = 1.6\,\mathrm{k\Omega}$, $R_{92} = 2.06\,\mathrm{k\Omega}$, $R_{112} = 2.75\,\mathrm{k\Omega}$, $R_{132} = 3.82\,\mathrm{k\Omega}$, $R_{152} = 5.75\,\mathrm{k\Omega}$, $R_{172} = 10.25\,\mathrm{k\Omega}$, $R_{192} = 32.75\,\mathrm{k\Omega}$.

2) When the number of scrolls is $2N+1$ ($N \geq 1$), one has $R_{i1}(2 \leq i \leq 19) = 1\,\mathrm{k\Omega}$, $R_{22} = 4.5\,\mathrm{k\Omega}$, $R_{42} = 4.19\,\mathrm{k\Omega}$, $R_{62} = 6.14\,\mathrm{k\Omega}$, $R_{82} = 6.5\,\mathrm{k\Omega}$, $R_{102} = 9.64\,\mathrm{k\Omega}$, $R_{122} = 12.5\,\mathrm{k\Omega}$, $R_{142} = 22.5\,\mathrm{k\Omega}$, $R_{162} = 66.5\,\mathrm{k\Omega}$, $R_{32} = 1.25\,\mathrm{k\Omega}$, $R_{52} = 1.60\,\mathrm{k\Omega}$, $R_{72} = 2.07\,\mathrm{k\Omega}$, $R_{92} = 2.75\,\mathrm{k\Omega}$, $R_{112} = 3.82\,\mathrm{k\Omega}$, $R_{132} = 5.75\,\mathrm{k\Omega}$, $R_{152} = 10.25\,\mathrm{k\Omega}$, $R_{172} = 32.75\,\mathrm{k\Omega}$.

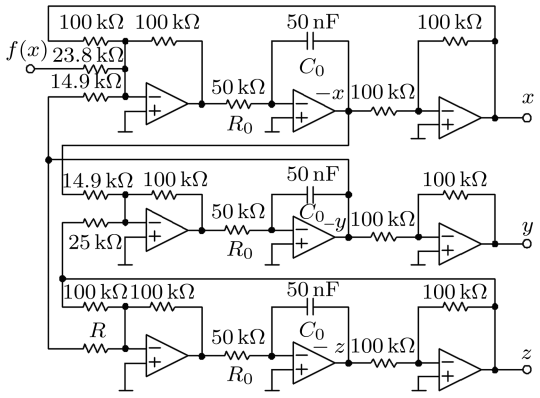

Fig.11. Module-based circuit design of multiple scroll chaotic system.

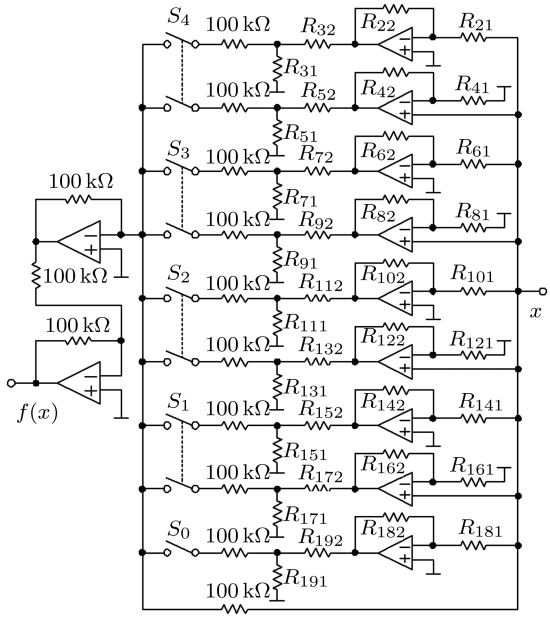

Fig.12. Circuit design of triangular wavefunction $f(x)$.

Table 7. Relationship among R, switch position and number of even scrolls.

S_0	S_1	S_2	S_3	S_4	$R/\,\mathrm{k\Omega}$	number of scrolls
on	off	off	off	off	5.6	2
on	on	off	off	off	7.6	4
on	on	on	off	off	8.0	6
on	on	on	on	off	8.3	8
on	on	on	on	on	8.4	10

Table 8. Relationship among R, switch position and number of odd scrolls.

S_0	S_1	S_2	S_3	S_4	$R/\,\mathrm{k\Omega}$	number of scrolls
off	on	off	off	off	7.0	3
off	on	on	off	off	8.0	5
off	on	on	on	off	8.4	7
off	on	on	on	on	8.55	9

5. Circuit experimental results

Based on the circuit design given in Figs.11 and 12 and Tables 7 and 8, the experimental results of 7, 8, 9, and 10-scroll chaotic attractors generated from triangular wave are shown in Fig.13.

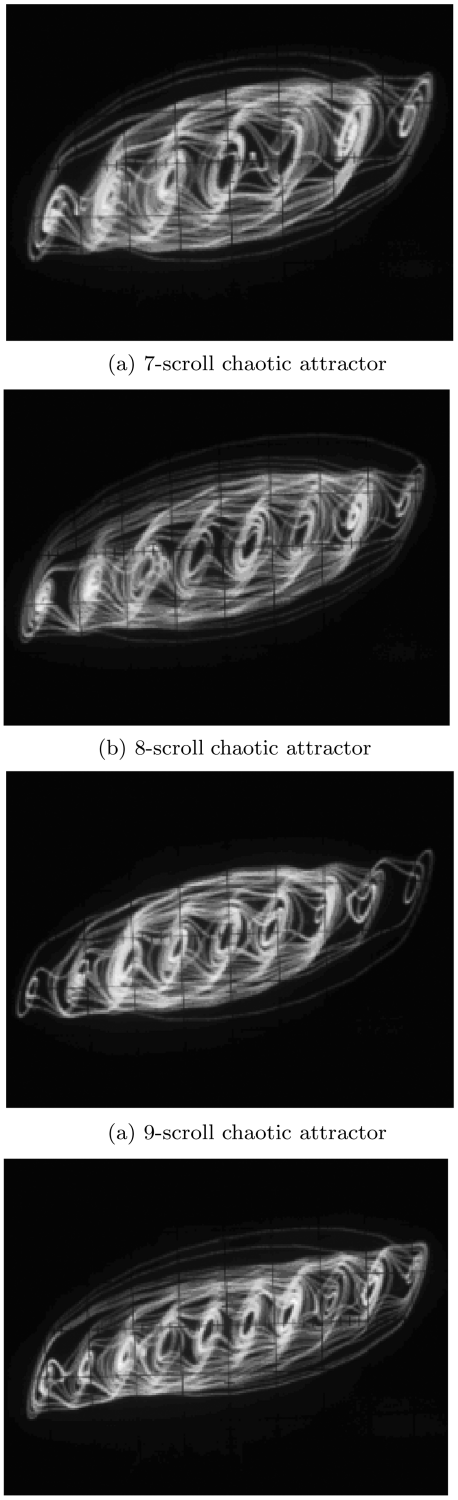

(a) 7-scroll chaotic attractor

(b) 8-scroll chaotic attractor

(a) 9-scroll chaotic attractor

(b) 10-scroll chaotic attractor

Fig.13. 7, 8, 9 and 10-scroll chaotic attractors obtained by circuit experiment.

6. Conclusions

In this paper, a novel multi-scroll chaotic system has been proposed. Theoretical design and numerical simulation confirm that three different types of multiple scroll chaotic attractors are available by constructing triangular wave, sawtooth wave and hysteresis sequence. It should be emphasized that the present novel system is different from the classical multiple scroll Chua system in several aspects: the dimensionless state equations, the nonlinear functions, the maximum Lyapunov exponents and the attractor's topology. Furthermore, some basic dynamical behaviours, such as equilibrium points, eigenvalues, eigenvectors, eigenplanes, bifurcations and Lyapunov exponents, are then further investigated, confirming the chaotic nature of the present new system. Based on dimensionless state equations and module-based method, the success of the design has been verified by circuit implementations, which is in good agreement with numerical simulations.

References

[1] Lorenz E N 1963 *J. Atmos. Sci.* **20** 130

[2] Stewart I 2002 *Nature* **406** 948

[3] Chen G R and Lü J H 2003 *Dynamics of the Lorenz System Family: Analysis, Control, and Synchronization* (Beijing: Science Press) (in Chinese)

[4] Chua L O, Komuro M and Matsumoto T 1986 *IEEE Trans. Circuits Syst.* I **33** 1072

[5] Elwakil A S and Kennedy M P 2001 *IEEE Trans. Circuits Syst.* I **48** 289

[6] Elwakil A S, Özoguz S and Kennedy M P 2002 *IEEE Trans. Circuits Syst.* I **49** 527

[7] Özoguz S, Elwakil A S and Kennedy M P 2002 *Int. J. Bifurc. Chaos* **12** 1627

[8] Yalcin M E, Suykens J A K and Vandewalle J 2000 *IEEE Trans. Circuits Syst.* I **47** 425

[9] Suykens J A K and Vandewalle J 1993 *IEEE Trans. Circuits Syst.* I **40** 861

[10] Tang K S, Zhong G Q and Chen G R 2001 *IEEE Trans. Circuits Syst.* I **48** 1369

[11] Zhong G Q, Man K F and Chen G R 2002 *Int. J. Bifurc. Chaos* **12** 2907

[12] Yu S M, Qiu S S and Lin Q H 2003 *Sci. Chin.* F **46** 104

[13] Yu S M, Ma Z G, Qiu S S and Lin Q H 2004 *Chin. Phys.* **13** 317

[14] Yu S M 2004 *Acta Phys. Sin.* **53** 4111 (in Chinese)

[15] Yu S M, Lü J H, Leung H and Chen G R 2005 *IEEE Trans. Circuits Syst.* I **52** 1459

[16] Yu S M, Lin Q H and Qiu S S 2004 *Acta Phys. Sin.* **53** 2084 (in Chinese)

[17] Yu S M, Lü J H and Chen G R 2007 *Chaos* **17** 013118

[18] Yu S M, Lü J H and Chen G R 2007 *IEEE Trans. Circuits Syst.* I **54** 2087

[19] Yu S M, Tang K S and Chen G R 2007 *Int. J. Bifurc. Chaos* **17** 3951

[20] Yalcin M E, Suykens J A K and Vandewalle J 2002 *Int. J. Bifurc. Chaos* **12** 23

[21] Lü J H, Yu S M, Leung H and Chen G R 2006 *IEEE Trans. Circuits Syst.* I **53** 149

[22] Yu S M 2005 *Acta Phys. Sin.* **54** 1500 (in Chinese)

[23] Lü J H, Chen G R, Yu X and Leung H 2004 *IEEE Trans. Circuits Syst.* I **51** 2476

[24] Lü J H, Han F, Yu X and Chen G 2004 *Automatica* **40** 1677

[25] Lü J H, Yu X and Chen G R 2003 *IEEE Trans. Circuits Syst.* I **50** 198

[26] Yu S M, Lü J H, Tang K S and Chen G R 2006 *Chaos* **16** 033126

[27] Lü J H and Chen G R 2006 *Int. J. Bifurc. Chaos* **16** 775

[28] Yu S M, Lü J H and Chen G R 2007 *Int. J. Bifurc. Chaos* **17** 1785